Direct Comparison of the Tau PET Tracers ^{18}F-Flortaucipir and ^{18}F-MK-6240 in Human Subjects

Alexandra Gogola[1], Davneet S. Minhas[1], Victor L. Villemagne[2], Ann D. Cohen[2], James M. Mountz[1], Tharick A. Pascoal[2], Charles M. Laymon[1,3], N. Scott Mason[1], Milos D. Ikonomovic[2,4], Chester A. Mathis[1], Beth E. Snitz[4], Oscar L. Lopez[4], William E. Klunk[2], and Brian J. Lopresti[1]

[1]Department of Radiology, University of Pittsburgh, Pittsburgh, Pennsylvania; [2]Department of Psychiatry, University of Pittsburgh, Pittsburgh, Pennsylvania; [3]Department of Bioengineering, University of Pittsburgh, Pittsburgh, Pennsylvania; and [4]Department of Neurology, University of Pittsburgh, Pittsburgh, Pennsylvania

Tau PET tracers exhibit varying levels of specific signal and distinct off-target binding patterns that are more diverse than amyloid PET tracers. This study compared 2 frequently used tau PET tracers, ^{18}F-flortaucipir and ^{18}F-MK-6240, in the same subjects. **Methods:** ^{18}F-flortaucipir and ^{18}F-MK-6240 scans were collected within 2 mo in 15 elderly subjects varying in clinical diagnosis and cognition. FreeSurfer, version 5.3, was applied to 3-T MR images to segment Braak pathologic regions (I–VI) for PET analyses. Off-target binding was assessed in the choroid plexus, meninges, and striatum. SUV ratio (SUVR) outcomes were determined over 80–100 min (^{18}F-flortaucipir) or 70–90 min (^{18}F-MK-6240) normalized to cerebellar gray matter. Masked visual interpretation of images was performed by 5 raters for both the medial temporal lobe and the neocortex, and an overall (majority) rating was determined. **Results:** Overall visual ratings showed complete concordance between radiotracers for both the medial temporal lobe and the neocortex. SUVR outcomes were highly correlated ($r^2 > 0.92$; $P \ll 0.001$) for all Braak regions except Braak II. The dynamic range of SUVRs in target regions was approximately 2-fold higher for ^{18}F-MK-6240 than for ^{18}F-flortaucipir. Cerebellar SUVs were similar for ^{18}F-MK-6240 and ^{18}F-flortaucipir, suggesting that differences in SUVRs are driven by specific signals. Apparent off-target binding was observed often in the striatum and choroid plexus with ^{18}F-flortaucipir and most often in the meninges with ^{18}F-MK-6240. **Conclusion:** Both ^{18}F-MK-6240 and ^{18}F-flortaucipir are capable of quantifying signal in a common set of brain regions that develop tau pathology in Alzheimer disease; these tracers perform equally well in visual interpretations. Each also shows distinct patterns of apparent off-target binding. ^{18}F-MK-6240 showed a greater dynamic range in SUVR estimates, which may be an advantage in detecting early tau pathology or in performing longitudinal studies to detect small interval changes.

Key Words: tau, PET, Alzheimer disease, ^{18}F-flortaucipir, ^{18}F-MK-6240

J Nucl Med 2022; 63:108–116
DOI: 10.2967/jnumed.120.254961

Alzheimer disease (AD) is pathologically characterized by 2 specific brain pathologies: extracellular β-amyloid (Aβ) plaques and intracellular neurofibrillary tangles (NFTs) comprised of hyperphosphorylated tau protein. Although much evidence supports the amyloid cascade hypothesis of AD (*1*), whereby abnormal Aβ deposition is an initiating feature of AD, tau pathology is more closely linked to symptom severity, rate of decline, and development of dementia in AD pathophysiologic spectrum patients (*2*) and to a decline in visuospatial and language functions (*3*).

The ability to detect tau pathology in the living brain is critical for understanding the relationship between neuropathology and clinical symptoms and for monitoring the efficacy of novel antitau therapies (*3–7*). In addition to the recently U.S Food and Drug Administration–approved flortaucipir (Tauvid; Eli Lilly and Co.), previously known as ^{18}F-AV-1451 and ^{18}F-T807 (*8*), several tau radioligands have been advanced to investigational human studies, including ^{18}F-MK-6240 (*9*), ^{18}F-THK-5317, ^{18}F-THK-5351, ^{11}C-PBB3, ^{18}F-RO-948, ^{18}F-PI-2620, ^{18}F-GTP1, and ^{18}F-PM-PBB3 (*4*). Ongoing investigations underscore that tau radioligands differ in specificity to species of tau aggregates, dynamic range, and nonspecific and off-target binding (*4*). Of the tau imaging agents under development, ^{18}F-flortaucipir and ^{18}F-MK-6240 have seen widespread investigational use and have emerged as leading candidates for clinical translation.

Flortaucipir shows high in vitro binding affinity and selectivity for paired helical filament tau (PHF-tau) constituting NFT pathology, and in vivo indices of tau load correlate well with postmortem AD-related tau pathology (*10*). In vivo patterns of ^{18}F-flortaucipir retention reflect Braak pathologic staging (*11*) and support PET-based staging of AD (*6*). A robust ^{18}F-flortaucipir in vivo signal is observed predominantly in patients who show AD-characteristic Aβ deposits (*4*). Data suggest that ^{18}F-flortaucipir is specific for the mixed 3- and 4-repeat (3R/4R) PHF-tau deposits prevalent in AD NFTs and dystrophic neurites (*4*) and suggest utility for differential diagnoses of AD from other tauopathies (*12*).

An autopsy confirmation study of ^{18}F-flortaucipir detected an advanced level of NFT pathology (Braak V–VI) and high levels of neuropathologic change according to the joint National Institute of Aging–Alzheimer Association criteria for an AD neuropathologic diagnosis (*10*). However, some ^{18}F-flortaucipir characteristics are not ideal for PET imaging assessments, such as slower clearance from the cortex than the cerebellum with increasing tau pathologic burden, resulting in unstable SUV ratio (SUVR) outcomes even after long periods (*13*). Off-target binding in the basal ganglia, choroid plexus, and other regions (*4*) may influence specific signal determination in adjacent regions. Although the test–retest reproducibility of ^{18}F-flortaucipir is excellent (<4%) (*14*), a low signal

Received Aug. 9, 2020; revision accepted Apr. 6, 2021.
For correspondence or reprints, contact Brian J. Lopresti (brianl@pitt.edu).
Published online Apr. 16, 2021.

in mild cognitive impairment (MCI) and early AD combined with high nonspecific retention in amyloid-negative controls may pose challenges for early detection and for longitudinal tracking of tau aggregation (*15*,*16*).

^{18}F-MK-6240 has also shown high affinity and selectivity for 3R/4R PHF-tau (*5*,*17*) and has advanced to human studies (*4*,*18*). In amyloid PET–positive subjects, ^{18}F-MK-6240 showed excellent brain uptake and retention patterns consistent with Braak stages of tau pathology (*4*,*18*). Like ^{18}F-flortaucipir, the slowly equilibrating kinetics of ^{18}F-MK-6240 may represent a source of bias in SUVR outcomes for typical scanning intervals (e.g., 70–90 min or 90–110 min) (*5*,*17*–*21*). Off-target binding of ^{18}F-MK-6240 is not present in the basal ganglia and choroid plexus (*17*,*18*,*21*), although off-target binding in the retina, ethmoid sinus, substantia nigra, and dura mater is common (*19*). In vivo studies of ^{18}F-MK-6240 show good reproducibility (test–retest reproducibility, $< 6\%$) (*18*,*22*), an ability to differentiate cognitively normal subjects from MCI or AD patients (*19*,*23*), and sensitivity for detecting tau in early disease stages (*21*).

Although amyloid PET tracers show similar patterns of specific signal across subjects and radiotracers, this is not the case for tau tracers. While both ^{18}F-flortaucipir and ^{18}F-MK-6240 appear to detect tau deposits in vivo, evaluating the relative performance of these 2 radiotracers is complicated by the absence of direct comparisons performed in the same subjects. This shortcoming layers biologic variability on top of tracer variability since there is a wide range in the spatial distribution and severity of tau pathology across individuals (*3*). The present work describes a direct comparison of ^{18}F-flortaucipir and ^{18}F-MK-6240 in a group of 15 subjects having a range of clinical diagnoses studied with both radiotracers within a 2-mo interval.

MATERIALS AND METHODS

Human Subjects

The study was approved by the University of Pittsburgh's Institutional Review Board, and all subjects or their caregivers consented to the Alzheimer Disease Research Center examination and imaging protocol. Fifteen subjects were recruited through the University of Pittsburgh Alzheimer Disease Research Center and other population-based studies (Table 1), selected to represent a range of AD pathologic burden based on cognition and amyloid PET. No subjects were excluded. All subjects underwent a battery of cognitive tests and a consensus clinical diagnosis performed by the same Alzheimer Disease Research Center neurologist, geriatric psychiatrist, and neuropsychologist (*24*). A ^{11}C-Pittsburgh compound B (^{11}C-PiB) scan was performed on the day of the ^{18}F-flortaucipir scan to determine amyloid status. Five subjects were clinically diagnosed with probable AD (mini-mental state examination score range, 9–29), and all were globally ^{11}C-PiB–positive. One subject was classified as MCI-amnestic (mini-mental state examination score, 22), but a negative ^{11}C-PiB scan suggested a non-AD etiology. The remaining 9 subjects had normal cognition (NC), although 6 scored outside the reference ranges on at least 1 objective measure of cognition, memory, or executive function (classified as "impaired test without complaints"). Among the 9 NC subjects, 7 had mini-mental state examination scores within reference ranges (*28*–*30*) and only 1 NC subject was globally ^{11}C-PiB–positive.

Imaging

^{11}C-PiB and ^{18}F-MK-6240 were produced in accordance with drug master files approved by the University of Pittsburgh Radioactive Drug Research Committee. Precursors for ^{18}F-flortaucipir and ^{18}F-MK-6240 were provided by Avid Radiopharmaceuticals, Inc., and Cerveau Technologies, Inc., respectively, under existing agreements. ^{18}F-flortaucipir was prepared in accordance with procedures detailed in Food and Drug Administration–approved investigational-new-drug application 123396, and ^{18}F-MK-6240 was prepared as previously described (*9*). ^{18}F-flortaucipir (340 ± 19 MBq) and ^{18}F-MK-6240 (189 ± 15 MBq) PET scans were collected within 26 ± 14 d (maximum, 54 d) on a Biograph mCT (TrueV) (Siemens Healthcare) and reconstructed as previously described (*25*). To assess amyloid status, ^{11}C-PiB scans (50–70 min, 529 ± 107 MBq) were collected on a Siemens ECAT HR+ on the same day as ^{18}F-flortaucipir scans (*26*). A sagittal T1-weighted MPRAGE (magnetization-prepared rapid acquisition with gradient echo) MR image was acquired using a 3.0T Siemens Prisma scanner (Siemens Healthcare) for brain segmentation and parcellation.

Data Analysis

MR images were processed using FreeSurfer, version 5.3, to obtain a brain parcellation atlas for PET image sampling as previously described (*25*,*27*). Briefly, motion-corrected ^{18}F-MK-6240 and ^{18}F-flortaucipir images were summed over 70–90 min for ^{18}F-MK-6240 (*21*) and 80–100 min for ^{18}F-flortaucipir (*13*,*28*) and registered to a subject-specific reference MR image. The FreeSurfer parcellation template was used to sample summed PET images, and a volume-weighted average of FreeSurfer regions was calculated for each of 6 composite Braak stage regions of interest (ROIs) (Supplemental Table 1; supplemental materials are available at http://jnm.snmjournals.org) (*11*). Striatal FreeSurfer ROIs (caudate, putamen, accumbens, and pallidum) were excluded from the composite Braak V ROI because of frequent off-target binding of ^{18}F-flortaucipir but were examined separately as a composite striatal region (bilateral), along with the choroid plexus (unilateral because of asymmetries) and meninges, to assess off-target binding (*5*). Regional ^{18}F-flortaucipir and ^{18}F-MK-6240 SUVRs and SUVR images were calculated using cerebellar gray matter as a reference (*19*,*29*).

To compare off-target binding in the meninges, individual MR images were normalized into Montreal Neurological Institute space using SPM12 software (Statistical Parametric Mapping, University College, London). The c4 ROI (meninges + bone) was extracted from the SPM12 tissue probability map and edited to exclude other head and neck tissues based on an average MRI of all 15 subjects (Supplemental Fig. 1). The c4 ROI was subsequently transformed back to native space for PET image sampling. Voxelwise comparisons of ^{18}F-flortaucipir and ^{18}F-MK-6240 SUVR images were performed using SPM12. T-value parametric maps (representing voxels for which ^{18}F-MK-6240 $>$ ^{18}F-flortaucipir and ^{18}F-flortaucipir $>$ ^{18}F-MK-6240) were generated from the output of the paired t test and overlaid on an MRI template for visualization.

Visual Assessments

^{18}F-flortaucipir and ^{18}F-MK-6240 SUVR images were visually assessed by 5 experienced raters using a randomized coding scheme. Ratings were performed using only the PET images, which were assessed for tau pathology in the medial temporal lobe (MTL) and neocortex (NEO). Interrater reliability (Fleiss κ) was assessed across tracers and regions. The overall MTL and NEO ratings for assessing radiotracer concordance were based on a simple majority of 5 individual ratings. Additional details are provided in the supplemental materials.

RESULTS

PET Imaging

^{18}F-flortaucipir and ^{18}F-MK-6240 PET SUVR images displayed a range of tau pathology, with patterns of cortical involvement that were primarily posterior (AD2, AD3), highly focal (AD1), or widespread (AD4) (Fig. 1). In NC subjects, the tau PET signal for both radiotracers was modest and most prominent in the MTL.

TABLE 1
Subject Characteristics

Subject no.	Age (y)	Sex	MMSE	Education (y)	Scan interval (d)	Diagnosis
AD1	83	M	20	16	2	Probable AD (atypical)
AD2	68	M	23	14	6	Probable AD
AD3	86	M	15	12	1	Probable AD
AD4	53	M	9	12	2	Probable AD
AD5	64	F	29	12	1	Probable AD
MCI1	77	M	22	12	20	MCI-amnestic + other
NC1	79	F	24	12	7	Abnormal w/o complaint
NC2	79	F	30	18	52	Normal cognition
NC3	79	F	28	14	54	Abnormal w/o complaint
NC4	76	F	30	14	48	Abnormal w/o complaint
NC5	76	M	22	11	26	Abnormal w/o complaint
NC6	73	F	30	18	24	Abnormal w/o complaint
NC7	82	F	30	14	30	Abnormal w/o complaint
NC8	75	F	30	14	19	Normal cognition
NC9	69	F	30	16	49	Normal cognition

MMSE = mini-mental state examination; w/o = without.

Visual Assessments

Five raters assessed abnormal tracer retention in the MTL and NEO for ^{18}F-flortaucipir and ^{18}F-MK-6240. Overall tau-positivity ratings showed complete concordance between radiotracers in the MTL and NEO (Table 2), and there was substantial agreement between raters ($\kappa > 0.73$) for both regions (MTL and NEO) and radiotracers (Table 3). Individual ratings showed complete agreement for all AD subjects and were least reliable in patients with low levels of tau pathology (e.g., NC4 and NC5, Supplemental Fig. 2).

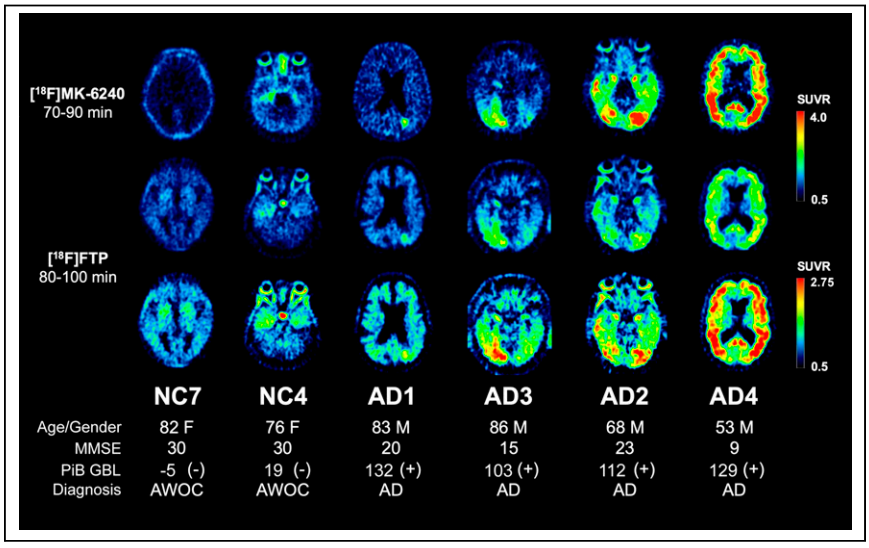

FIGURE 1. ^{18}F-flortaucipir (^{18}F-FTP) and ^{18}F-MK-6240 SUVR images from 6 subjects representing the range of tau pathology observed in our cohort. From left to right: subject showing no evidence of tau pathology (NC7); cognitively normal subject showing early Braak stage pathology (NC4); atypical AD subject with tau pathology in MTL and evidence of focal uptake in Braak V (AD1); and 3 AD subjects showing progression of increasingly severe tau pathology culminating in widespread neocortical involvement in AD4. ^{18}F-flortaucipir and ^{18}F-MK-6240 are shown on common scale (SUVR, 0.5–4.0). ^{18}F-FTP images are repeated (row 3) on compressed scale (SUVR, 0.5–2.75) so that subtle differences may be more appreciated. AWOC = abnormal without complaint; GBL = global; MMSE = mini-mental state examination.

SUVR Analyses

^{18}F-flortaucipir and ^{18}F-MK-6240 SUVRs correlated strongly ($r^2 > 0.9$; $p \ll 0.001$) across Braak stage regions (Fig. 2 except for Braak II ($r^2 = 0.52$; $P = 0.0024$). However, the dynamic range of SUVR, as indicated by the regression slope, was approximately 2-fold greater for ^{18}F-MK-6240 across Braak stage regions except Braak II, where the difference was more modest ($\times 1.4$). The distributions of cerebellar gray matter SUVs did not significantly differ between ^{18}F-flortaucipir and ^{18}F-MK-6240 ($P > 0.4$, paired t test), with a mean cerebellar SUV of 0.88 ± 0.18 and 0.84 ± 0.16, respectively (Fig. 2, right).

Off-Target Binding

Figure 3 shows the distribution of SUVR outcomes and representative images of typical off-target binding, where the striatum and choroid plexus were frequent loci of ^{18}F-flortaucipir off-target signal. By comparison, off-target binding of ^{18}F-MK-6240 in these regions was low. Off-target binding of ^{18}F-flortaucipir in the choroid plexus was frequent but variable, with an elevated signal (SUVR > 1.0 in either hemisphere) being seen in 9 of 15 subjects and extreme

TABLE 2
Visual Assessments of ^{18}F-Flortaucipir and ^{18}F-MK-6240 Scans

	MTL		NEO		PiB GBL		
Subject no.	FTP	MK	FTP	MK	SUVR	Centiloids	Aβ status
AD1	POS	POS	POS	POS	2.53	132	POS
AD2	POS	POS	POS	POS	2.42	112	POS
AD3	POS	POS	POS	POS	2.3	103	POS
AD4	POS	POS	POS	POS	2.47	129	POS
AD5	POS	POS	POS	POS	2.51	121	POS
MCI1	POS	POS	NEG	NEG	1.24	0	NEG
NC1	POS	POS	POS	POS	1.56	50	POS
NC2	NEG	NEG	NEG	NEG	1.13	−2	NEG
NC3	NEG	NEG	NEG	NEG	1.13	−10	NEG
NC4	POS	POS	POS	POS	1.31	19	NEG
NC5	NEG	NEG	NEG	NEG	1.14	4	NEG
NC6	NEG	NEG	NEG	NEG	1.18	9	NEG
NC7	NEG	NEG	NEG	NEG	1.16	−5	NEG
NC8	NEG	NEG	NEG	NEG	1.21	4	NEG
NC9	NEG	NEG	NEG	NEG	1.29	6	NEG

FTP = ^{18}F-flortaucipir; MK = ^{18}F-MK-6240; POS = positive; NEG = negative.

values (SUVR > 2) being seen in 1 subject (NC5) who was amyloid-negative and tau-negative in the MTL and NEO by visual assessment. The remaining ^{18}F-flortaucipir images and all ^{18}F-MK-6240 images showed low off-target binding in the choroid plexus. In the striatum, off-target binding of ^{18}F-flortaucipir was approximately 56% higher than that of ^{18}F-MK-6240 on average (SUVR, 1.45 ± 0.12 vs. 0.93 ± 0.18), and the ranges of striatal SUVRs for the 2 tracers overlapped in only 3 of 15 subjects (Fig. 3). Six of 15 subjects showed an increased ^{18}F-MK-6240 signal (SUVR > 1.0) at the pial surface of the brain, centered on the meninges (Fig. 3), although meningeal SUVR outcomes correlated strongly ($r^2 = 0.68$; $P < 0.001$) between tracers.

In another group of 6 subjects, all female, we noted a conspicuous signal from both radiotracers arising from an overgrowth of bony tissue on the internal surface of the calvarium, consistent with hyperostosis frontalis interna (*30*), which was apparent on CT and MR images (Fig. 4). Hyperostosis is a common benign radiographic finding in postmenopausal women (*31*) and is considered to be an X-chromosome–linked abnormality (*32*). In some subjects, CT scans revealed other sites of calcification or ossification corresponding to areas of increased ^{18}F-MK-6240 and ^{18}F-flortaucipir off-target signal; these sites included the pineal gland, the meninges of the falx cerebri, and other focal meningeal calcifications. These features were sometimes noted in the absence of more generalized meningeal ^{18}F-MK-6240 off-target binding, as in NC1 and NC4 (Fig. 4).

TABLE 3
Assessments of Interrater Reliability of Visual Ratings

Region	Tracer	κ	*z* score	*P*
MTL	FTP	0.836 (0.675–0.997)	10.2	<<0.0001
	MK	0.813 (0.653–0.973)	9.96	<<0.0001
NEO	FTP	0.733 (0.573–0.893)	8.98	<<0.0001
	MK	0.760 (0.600–0.920)	9.3	<<0.0001
All	FTP	0.785 (0.672–0.898)	13.6	<<0.0001
	MK	0.787 (0.674–0.900)	13.6	<<0.0001

κ = Fleiss κ-statistic.
Data in parentheses are 95% CIs.

Voxel-Based Analyses

T-value maps comparing patterns of ^{18}F-flortaucipir and ^{18}F-MK-6240 retention are shown in Figure 5 and reflect off-target binding patterns. Clusters of voxels in which ^{18}F-flortaucipir retention was significantly greater than ^{18}F-MK-6240 retention were evident in the striatum, brain stem, and subcortical and cerebellar white matter (Fig. 5A). The voxels in which ^{18}F-MK-6240 retention was significantly greater than ^{18}F-flortaucipir retention were limited to the meninges and bone (Fig. 5B). Clusters of significant voxels in the cortical gray matter where tau pathology was concentrated were not observed in either direction.

DISCUSSION

Amyloid radiotracers in human subjects with typical AD dementia show a consistent pattern of pathology across tracers and subjects despite differences in dynamic signal range and nonspecific binding characteristics (*33–36*). The similarity in the brain distribution of specific signal between Aβ radiotracers has facilitated standardization techniques, such as centiloid scaling (*37*,*38*), and is likely attributable to a single human isoform of fibrillar Aβ constituting a distinct brain pathology—amyloid plaques—which is the dominant signal source for Aβ in vivo imaging agents (*39*,*40*). Tau is considerably more complex, with 6 human

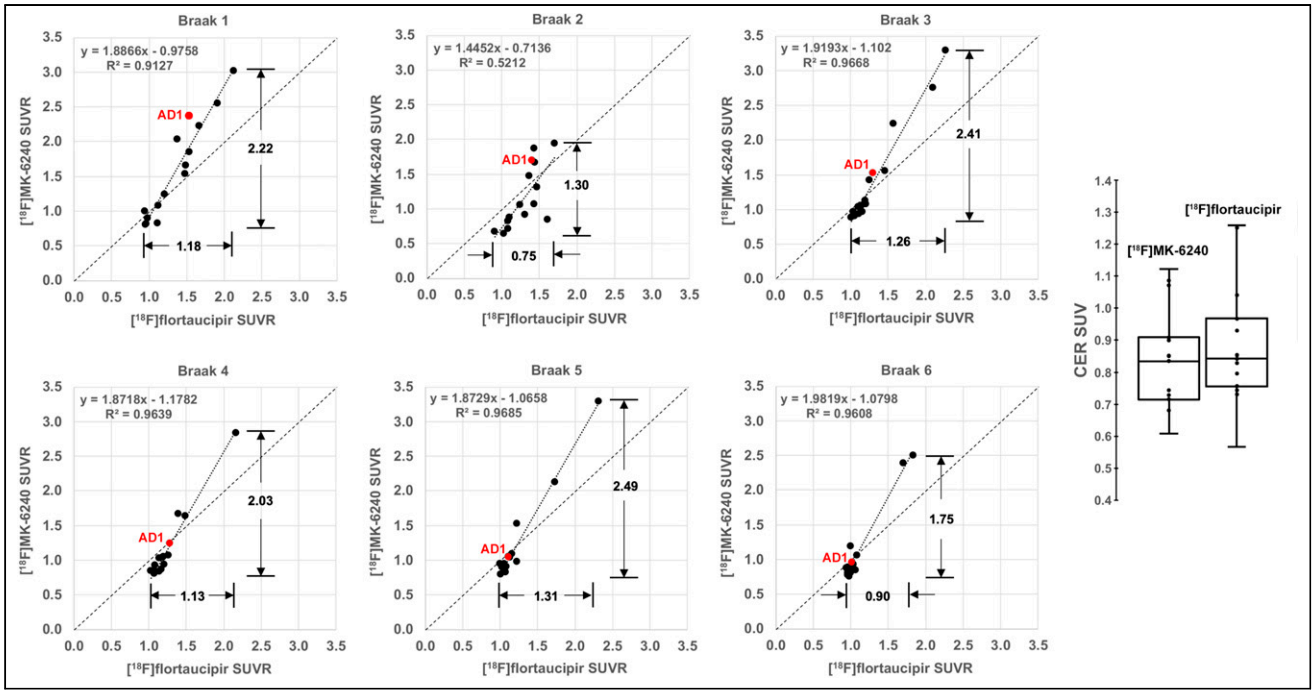

FIGURE 2. Comparison of ^{18}F-flortaucipir and ^{18}F-MK-6240 SUVR outcomes across 6 Braak stage regions, showing linear regression of values. For each Braak stage region, dynamic range of SUVR outcomes is indicated. Data point representing AD1 is shown to illustrate dilution of visually evident focal tau signal in large Braak-stage regions. CER = cerebellum.

isoforms, more posttranslational modifications, and a greater diversity of pathologic lesions (e.g., NFTs, astroglial and oligodendroglial tau inclusions, or Pick bodies), stages of tangle maturity (*41*), and ultrastructural conformations (i.e., PHF, straight filaments, or twisted filaments), although in AD the most prevalent species are NFTs comprising a PHF combination of 3R and 4R tau isoforms (*42*,*43*). In vitro binding studies of flortaucipir and MK-6240 suggest low affinity to tau pathologies other than PHF-tau (*17*,*29*,*44*–*46*), although a few in vivo imaging studies have suggested a possible or weak sensitivity of ^{18}F-flortaucipir to 4R-tau deposits in some primary tauopathies (*47*–*49*).

As suggested by autoradiography (*44*), the present study suggested that ^{18}F-flortaucipir and ^{18}F-MK-6240 are almost certainly detecting the same AD- and age-related tau pathology. This

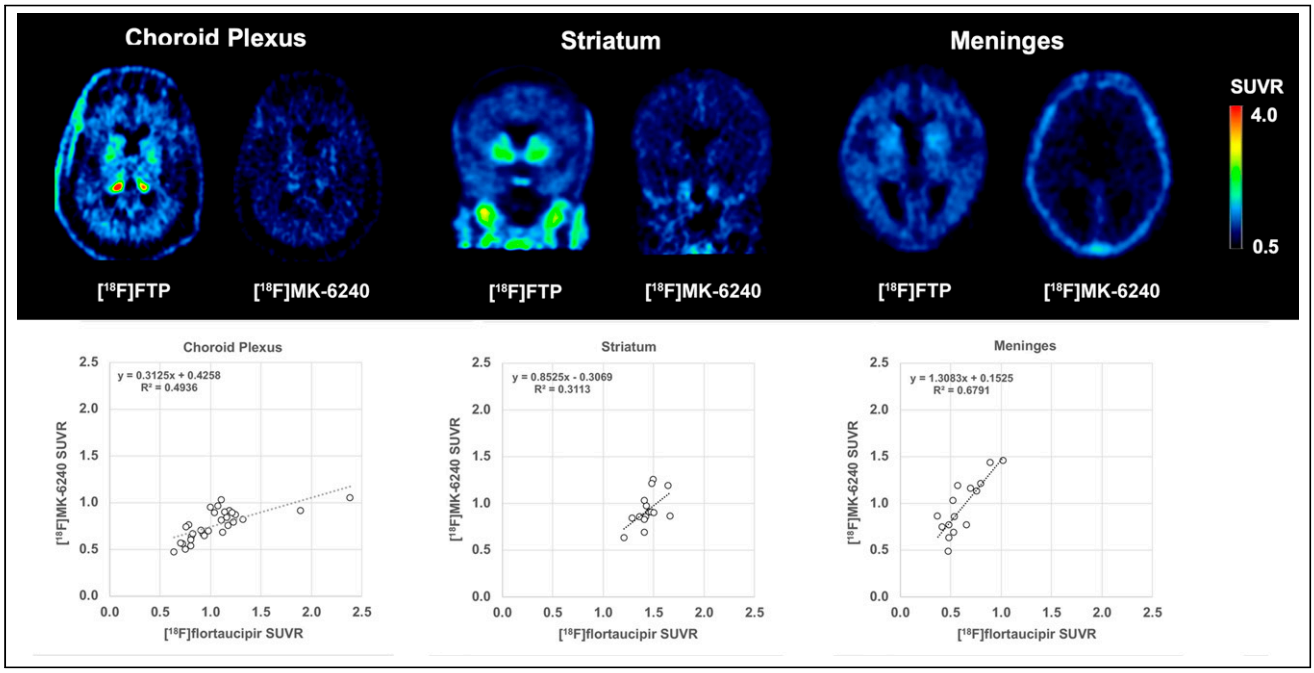

FIGURE 3. Comparison of off-target binding of ^{18}F-flortaucipir (^{18}F-FTP) and ^{18}F-MK-6240 in choroid plexus, striatum, and meninges. Shown are representative images of typical patterns of off-target retention in these regions (top). Distribution of SUVR outcomes is also shown (below).

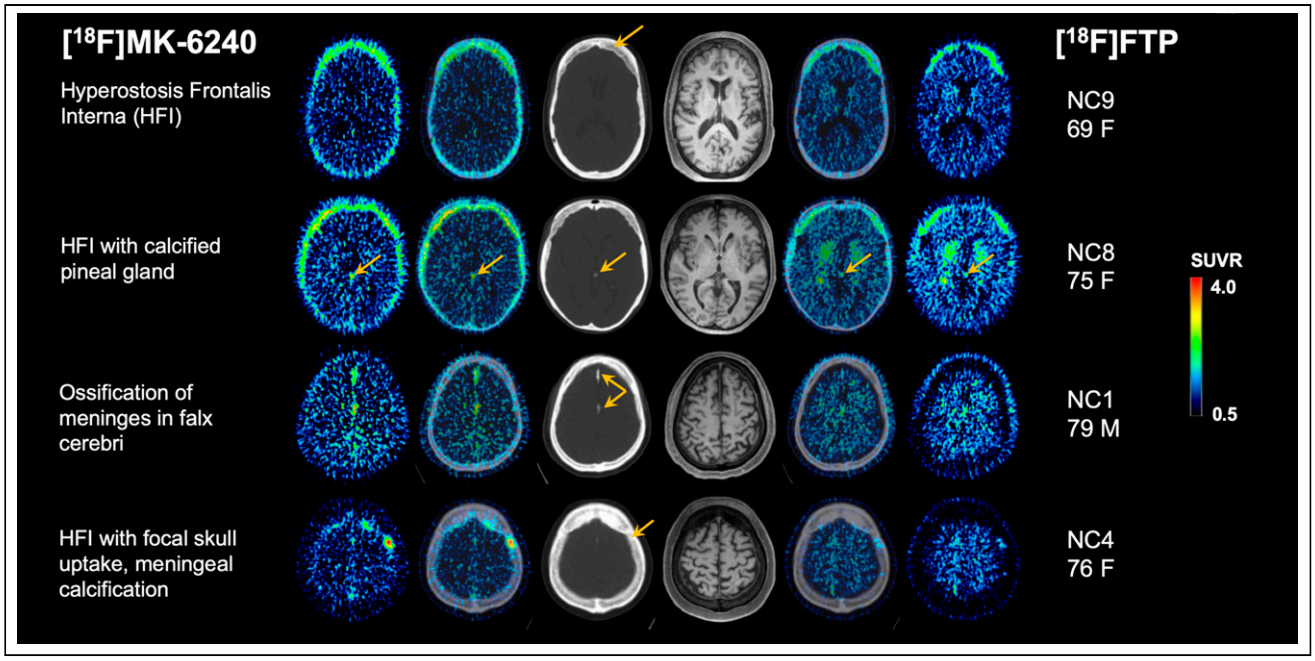

FIGURE 4. ^{18}F-flortaucipir (^{18}F-FTP), ^{18}F-MK-6240, CT, and MR images of subjects with hyperostosis frontalis interna (HFI) (first row); HFI and highly calcified pineal gland (second row); marked meningeal ossification and calcification in falx cerebri (third row); and HFI and bony lesion of skull with several small meningeal calcifications (fourth row).

possibility is evidenced by the similarity in radiotracer retention patterns across a spectrum of disease (Fig. 1), highly correlated SUVR outcomes across Braak stage regions, and voxel-based analyses that show no differences in patterns of specific binding to pathologic tau deposits (Fig. 5). In some Braak regions, we observed a slightly elevated floor signal for ^{18}F-flortaucipir compared with ^{18}F-MK-6240, suggesting the former to have a slightly higher nonspecific retention. This was most apparent in Braak II, as is likely attributable to spill-in from off-target binding of ^{18}F-flortaucipir in the choroid plexus.

Our approach to visual interpretation of ^{18}F-flortaucipir and ^{18}F-MK-6240 images was intended to mirror a clinical nuclear medicine environment, albeit with slightly more granularity than a global rating. Although we observed only 1 instance in our small cohort in which a subject (MCI1) was adjudicated overall to be positive in either the MTL or the NEO but not both, conceivably distinct ratings for MTL and NEO tau signal may provide some differentiation of the diverse tau phenotypes previously described (*3*) and, considering Aβ status, may help to differentiate AD pathology from normal aging processes (e.g., primary age-related tauopathy) characterized by MTL tau deposits that may occur independently of Aβ (*50*,*51*).

Although we observed differences in dynamic signal range and off-target binding between tracers, we expected either would perform well in visual assessments, in which off-target binding can be more easily accounted for. This expectation was supported by our results, which showed complete concordance between tracers in overall ratings for both the MTL and the NEO (Table 2) and substantial agreement between raters ($\kappa > 0.73$, Table 3), regardless of tracer or region.

Comparing visual assessments with diagnoses, both MTL and NEO tau pathology was present in all AD subjects. Among NC subjects, 7 of 9 showed no evidence of tau pathology in either the MTL or the NEO, whereas NC1 and NC4 were positive in both and had the highest ^{11}C-PiB SUVRs of all NC subjects, although only NC1 was quantitatively Aβ-positive (^{11}C-PiB CL = 50). The MCI subject, who was Aβ-negative (^{11}C-PiB CL = 0), was tau-positive only in MTL. This subject may be an example of primary age-related tauopathy.

Comparison of SUVR images shows that both ^{18}F-flortaucipir and ^{18}F-MK-6240 indicated the same tau pathology, although ^{18}F-MK-6240 showed a nearly 2-fold higher dynamic range (Fig. 2) as indexed by regression slopes ranging from 1.45 to 1.98. A similarity between ^{18}F-flortaucipir and ^{18}F-MK-6240 in cerebellar

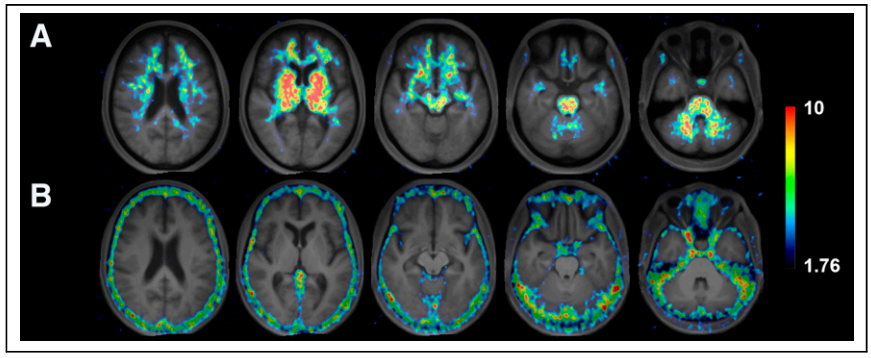

FIGURE 5. Voxel-based comparison of ^{18}F-flortaucipir and ^{18}F-MK-6240 retention. Shown are T-maps of significant contrasts ($P < 0.05$, uncorrected [$T > 1.76$]), where ^{18}F-FTP > ^{18}F-MK-6240 (A) and ^{18}F-MK-6240 > ^{18}F-FTP (B). T-maps are shown overlaid on average MR image generated from 15 subjects.

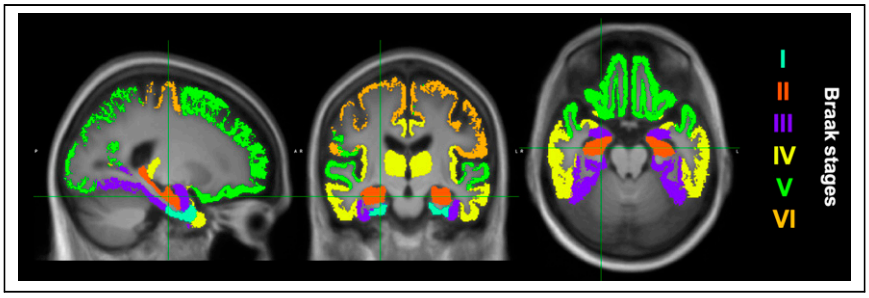

FIGURE 6. Grouping of FreeSurfer regions to correspond to Braak pathologic stages (I–VI).

gray matter SUVs, which are used to compute SUVR, indicated that this observation is not attributable to differences in nonspecific retention. In vitro saturation binding studies of ^{3}H-MK-6240 and ^{3}H-flortaucipir conducted using the same AD tissue homogenates showed ^{3}H-MK-6240 to have a 3- to 10-fold higher affinity (K_D) for PHF-tau than did ^{3}H-flortaucipir, as well as a 3- to 5-fold higher B_{max}/K_D ratio (*17*,*46*). Indeed, differences in the pharmacologic properties may reasonably explain the increased dynamic range of ^{18}F-MK-6240 SUVR, although other factors such as nonspecific binding, radiotracer metabolism, and rates of plasma and reference region clearance may influence in vivo specific binding measures. Although both tracers appeared to be well suited to visual interpretation, the greater dynamic range of ^{18}F-MK-6240 may represent an advantage for longitudinal studies of tau progression or treatment response, in which detecting small interval changes is key.

An examination of the dispersion of the SUVR data (Fig. 2) shows that for all regions except Braak II there was a subject cluster, with SUVRs of approximately 1 for both radiotracers in all subjects visually adjudicated to be negative, whereas the positive cases covered a much broader range, with few subjects overlapping with the negative cluster. The fact that there were only a few visually positive subjects with low SUVRs likely indicates that they represent subjects for whom the raters identified focally intense radiotracer uptake but that the focus of increased signal was diluted in the averaging of all voxels in the respective Braak stage region, such as the relatively large Braak III–VI regions shown in Figure 6. An example of such a subject is AD1 (Fig. 1), who showed a clear unilateral focus of increased uptake in the left precuneus that, by visual ratings, was indicated as positive for the MTL and NEO with both radiotracers, but ^{18}F-flortaucipir and ^{18}F-MK-6240 SUVRs for the Braak V region in this subject were only 1.16 and 1.09. This example highlights a potential limitation of sampling PET images of tau radiotracers in accordance with Braak staging. Another complication is that in some elderly subjects with or without cognitive impairment, significant MTL (Braak stage I–III region) pathology may occur independently of Aβ. These subjects may represent cases of primary age-related tauopathy. Therefore, classifying tau status (T+/T−) on the basis of MTL pathology alone would presumably reduce the specificity of a pathologic diagnosis of AD. It is likely that the most sensitive and specific indicators of tau lesions consistent with AD neuropathologic change will require tau PET positivity beyond MTL structures. However, the Braak IV region is relatively large and potentially suffers from the limitation of diluting a focal signal that might be the earliest indicator of neocortical spread of tau pathology. For this reason, others have moved toward a data-driven approach with a more granular tissue sampling strategy (*52*).

^{18}F-flortaucipir images often exhibit elevated off-target binding in the striatum and choroid plexus (Fig. 4), as well as other tissues, which may occur independently of neurodegenerative disease pathology as previously reported (*6*). For ^{18}F-MK-6240, the frequent observation of elevated signal arising from the meninges and other extracerebral structures (Fig. 3) was in accordance with previous observations (*21*). In some cases, it was apparent that spill-in of off-target ^{18}F-MK-6240 signal from the meninges could impact the quantification of signal in cortical brain regions as well as the cerebellum, although the fact that meningeal off-target signal is not apparent on ^{18}F-flortaucipir images yet the SUVR outcomes of ^{18}F-flortaucipir and ^{18}F-MK-6240 correlated strongly (Fig. 2) suggests that this effect does not represent a major confounder.

The off-target signal in bone observed with both tracers, most notably in female subjects with hyperostosis frontalis interna, does not appear to be completely explained by in vivo defluorination of these tracers, as we did not observe widespread bone uptake consistent with ^{18}F-fluoride scans and the inspection of batch records from our ^{18}F-MK-6240 radiosyntheses did not show evidence of significant residual ^{18}F-fluoride in the injectate. Intracranial calcifications are a common and normal age-related radiographic finding, often described in the pineal gland, habenula, choroid plexus, basal ganglia, falx cerebri, dura mater, petroclinoid ligaments, superior sagittal sinus, and dentate nuclei of the cerebellum and the hippocampus (*53*). Interestingly, these regions overlap areas where off-target binding of these tau radiotracers is often observed, but inspection of low-dose CT scans showed no macroscopic calcifications in the choroid plexus of our study subjects.

Limitations of the present study include a small sample size and a limited range of pathology and degree of clinical impairment. Only 1 of 9 NC subjects was globally amyloid positive and the only MCI subject was amyloid negative. The 5 AD subjects showed mild to moderate cognitive impairment, and we observed relatively limited tau pathology in Braak stages V and VI across the sample. Given the small sample size of our pathologically heterogeneous cohort, in which patients with advanced tau pathology comprise over one third of the study cohort, it might not be possible to generalize our measures of interrater reliability to other subject cohorts. We would expect there to be considerably less agreement and lower reliability in studies of cohorts that comprised predominantly cognitively normal elderly individuals, in whom tau burden is less. Indeed, we observed some discordance between raters among nondemented subjects (Supplemental Fig. 4). In our study, ^{18}F-MK-6240 injected doses were limited to 185 MBq to meet the organ dosimetry limits of the University of Pittsburgh's Radioactive Drug Research Committee. Another limitation of the present study was the lack of measures of intrarater reliability, as the small size and high disease burden in our cohort would be expected to yield a high level of intrarater reliability that also could not be generalized to other cohorts.

CONCLUSION

The direct comparison of brain distribution, specific signal, and off-target binding of ^{18}F-flortaucipir and ^{18}F-MK-6240 in the same subjects suggests that these tau radiotracers indicate the same tau

pathology and reflect Braak stages of NFT pathology. The off-target binding pattern was frequently observed in the choroid plexus and striatum for ^{18}F-flortaucipir and in the meninges for ^{18}F-MK-6240. Complete concordance in visual ratings of tau positivity suggests that both radiotracers can be expected to perform well for visual interpretation of images, although studies on larger cohorts across the entire spectrum of tau accumulation are needed to test the limits of visual rating methods. Differential ratings for the MTL and NEO may be useful for discriminating tau AD phenotypes and for differentiating AD neuropathologic changes from age-related tau deposition, although this methodology will also require further study. We observed ^{18}F-MK-6240 to have an approximately 2-fold greater dynamic range in specific signal across the range of pathology present in our subject cohort, possibly because of its higher affinity to PHF-tau. This may be an important consideration in planning longitudinal studies in which detecting small changes in tau load indices over relatively short periods is of paramount importance.

DISCLOSURE

GE Healthcare holds a license agreement with the University of Pittsburgh based on some of the technology described in this article. William Klunk and Chester Mathis are coinventors of ^{11}C-PiB and, as such, have a financial interest in this license agreement. Milos Ikonomovic received research funding from GE Healthcare. This work was supported by grants from the National Institute of Aging: AG025204 and AG005133. No other potential conflict of interest relevant to this article was reported.

ACKNOWLEDGMENTS

We thank the staff of the University of Pittsburgh PET Facility and the Alzheimer's Disease Research Center for their assistance.

KEY POINTS

QUESTION: What are the cross-sectional differences in on- and off-target binding of the two most commonly used tau PET imaging agents?

PERTINENT FINDINGS: The head-to-head comparison of ^{18}F-flortaucipir and ^{18}F-MK-6240 showed very similar relative levels of radiotracer retention in most cortical regions in both tau-negative and tau-positive cases, suggesting that these agents have on-target binding similar to that of PHF tau, the prevalent form in AD. However, there were important differences in off-target binding characteristics in the choroid plexus, striatum, and meninges.

IMPLICATIONS FOR PATIENT CARE: These tau PET imaging agents provide similar estimations of the presence of PHF tau related to AD, but care must be taken to understand the influence of off-target binding in the interpretation of each specific tracer.

REFERENCES

1. Hardy JA, Higgins GA. Alzheimer's disease: the amyloid cascade hypothesis. *Science.* 1992;256:184–185.
2. Schöll M, Lockhart SN, Schonhaut DR, et al. PET imaging of tau deposition in the aging human brain. *Neuron.* 2016;89:971–982.
3. Ossenkoppele R, Schonhaut DR, Scholl M, et al. Tau PET patterns mirror clinical and neuroanatomical variability in Alzheimer's disease. *Brain.* 2016;139:1551–1567.
4. Leuzy A, Chiotis K, Lemoine L, et al. Tau PET imaging in neurodegenerative tauopathies: still a challenge. *Mol Psychiatry.* 2019;24:1112–1134.
5. Saint-Aubert L, Lemoine L, Chiotis K, Leuzy A, Rodriguez-Vieitez E, Nordberg A. Tau PET imaging: present and future directions. *Mol Neurodegener.* 2017;12: 19.
6. Johnson KA, Schultz A, Betensky RA, et al. Tau positron emission tomographic imaging in aging and early Alzheimer disease. *Ann Neurol.* 2016;79:110–119.
7. Villemagne VL, Doré V, Bourgeat P, et al. Aβ-amyloid and tau imaging in dementia. *Semin Nucl Med.* 2017;47:75–88.
8. Chien DT, Bahri S, Szardenings AK, et al. Early clinical PET imaging results with the novel PHF-tau radioligand ^{18}F-T807. *J Alzheimers Dis.* 2013;34:457–468.
9. Walji AM, Hostetler ED, Selnick H, et al. Discovery of 6-(fluoro-^{18}F)-3-(^{1}H-pyrrolo[2,3-C]pyridin-1-yl)isoquinolin-5-amine (^{18}F-MK-6240): a positron emission tomography (PET) imaging agent for quantification of neurofibrillary tangles (NFTs). *J Med Chem.* 2016;59:4778–4789.
10. Fleisher AS, Pontecorvo MJ, Devous MD Sr, et al. Positron emission tomography imaging with ^{18}F-flortaucipir and postmortem assessment of Alzheimer disease neuropathologic changes. *JAMA Neurol.* 2020;77:829–839.
11. Braak H, Braak E. Staging of Alzheimer's disease-related neurofibrillary changes. *Neurobiol Aging.* 1995;16:271–278.
12. Ossenkoppele R, Rabinovici GD, Smith R, et al. Discriminative accuracy of ^{18}F-flortaucipir positron emission tomography for Alzheimer disease vs other neurodegenerative disorders. *JAMA.* 2018;320:1151–1162.
13. Shcherbinin S, Schwarz AJ, Joshi A, et al. Kinetics of the tau PET tracer ^{18}F-AV-1451 (T807) in subjects with normal cognitive function, mild cognitive impairment, and Alzheimer disease. *J Nucl Med.* 2016;57:1535–1542.
14. Devous MD Sr, Joshi AD, Navitsky M, et al. Test-retest reproducibility for the tau PET imaging agent flortaucipir F 18. *J Nucl Med.* 2018;59:937–943.
15. Zhao Q, Liu M, Ha L, Zhou Y; Alzheimer's Disease Neuroimaging Initiative. Quantitative ^{18}F-AV1451 brain tau PET imaging in cognitively normal older adults, mild cognitive impairment, and Alzheimer's disease patients. *Front Neurol.* 2019;10:486.
16. Baker SL, Harrison TM, Maass A, La Joie R, Jagust WJ. Effect of off-target binding on ^{18}F-flortaucipir variability in healthy controls across the life span. *J Nucl Med.* 2019;60:1444–1451.
17. Hostetler ED, Walji AM, Zeng Z, et al. Preclinical characterization of ^{18}F-MK-6240, a promising PET tracer for in vivo quantification of human neurofibrillary tangles. *J Nucl Med.* 2016;57:1599–1606.
18. Lohith TG, Bennacef I, Vandenberghe R, et al. Brain imaging of Alzheimer dementia patients and elderly controls with ^{18}F-MK-6240, a PET tracer targeting neurofibrillary tangles. *J Nucl Med.* 2019;60:107–114.
19. Pascoal TA, Shin M, Kang MS, et al. In vivo quantification of neurofibrillary tangles with ^{18}F-MK-6240. *Alzheimers Res Ther.* 2018;10:74.
20. Guehl NJ, Wooten DW, Yokell DL, et al. Evaluation of pharmacokinetic modeling strategies for in-vivo quantification of tau with the radiotracer ^{18}F-MK-6240 in human subjects. *Eur J Nucl Med Mol Imaging.* 2019;46:2099–2111.
21. Betthauser TJ, Cody KA, Zammit MD, et al. In vivo characterization and quantification of neurofibrillary tau PET radioligand ^{18}F-MK-6240 in humans from Alzheimer disease dementia to young controls. *J Nucl Med.* 2019;60:93–99.
22. Salinas C, Lohith TG, Purohit A, et al. Test-retest characteristic of ^{18}F-MK-6240 quantitative outcomes in cognitively normal adults and subjects with Alzheimer's disease. *J Cereb Blood Flow Metab.* 2020;40:2179–2187.
23. Pascoal TA, Therriault J, Benedet AL, et al. ^{18}F-MK-6240 PET for early and late detection of neurofibrillary tangles. *Brain.* 2020;143:2818–2830.
24. Jack CR Jr, Albert MS, Knopman DS, et al. Introduction to the recommendations from the National Institute on Aging-Alzheimer's Association workgroups on diagnostic guidelines for Alzheimer's disease. *Alzheimers Dement.* 2011;7:257–262.
25. Okonkwo DO, Puffer RC, Minhas DS, et al. ^{18}F-FDG, ^{11}C-PIB, and ^{18}F-AV-1451 PET imaging of neurodegeneration in two subjects with a history of repetitive trauma and cognitive decline. *Front Neurol.* 2019;10:831.
26. McNamee RL, Yee SH, Price JC, et al. Consideration of optimal time window for Pittsburgh compound-B PET summed uptake measurements. *J Nucl Med.* 2009;50:348–355.
27. Fischl B, van der Kouwe A, Destrieux C, et al. Automatically parcellating the human cerebral cortex. *Cereb Cortex.* 2004;14:11–22.
28. Baker SL, Lockhart SN, Price JC, et al. Reference tissue-based kinetic evaluation of ^{18}F-AV-1451 for tau imaging. *J Nucl Med.* 2017;58:332–338.
29. Marquié M, Normandin MD, Vanderburg CR, et al. Validating novel tau positron emission tomography tracer ^{18}F-AV-1451 (T807) on postmortem brain tissue. *Ann Neurol.* 2015;78:787–800.
30. She R, Szakacs J. Hyperostosis frontalis interna: case report and review of literature. *Ann Clin Lab Sci.* 2004;34:206–208.
31. May H, Peled N, Dar G, Abbas J, Hershkovitz I. Hyperostosis frontalis interna: what does it tell us about our health? *Am J Hum Biol.* 2011;23:392–397.

32. Hershkovitz I, Greenwald C, Rothschild BM, et al. Hyperostosis frontalis interna: an anthropological perspective. *Am J Phys Anthropol.* 1999;109:303–325.
33. Landau SM, Thomas BA, Thurfjell L, et al. Amyloid PET imaging in Alzheimer's disease: a comparison of three radiotracers. *Eur J Nucl Med Mol Imaging.* 2014; 41:1398–1407.
34. Wolk DA, Zhang Z, Boudhar S, Clark CM, Pontecorvo MJ, Arnold SE. Amyloid imaging in Alzheimer's disease: comparison of florbetapir and Pittsburgh compound-B positron emission tomography. *J Neurol Neurosurg Psychiatry.* 2012;83:923–926.
35. Morbelli S, Bauckneht M. Amyloid PET imaging: standardization and integration with other Alzheimer's disease biomarkers. *Methods Mol Biol.* 2018;1750: 203–212.
36. Villemagne VL, Mulligan RS, Pejoska S, et al. Comparison of ^{11}C-PIB and ^{18}F-florbetaben for Abeta imaging in ageing and Alzheimer's disease. *Eur J Nucl Med Mol Imaging.* 2012;39:983–989.
37. Whittington A, Gunn RN; Alzheimer's Disease Neuroimaging Initiative. Amyloid load: a more sensitive biomarker for amyloid imaging. *J Nucl Med.* 2019; 60:536–540.
38. Klunk WE, Koeppe RA, Price JC, et al. The centiloid project: standardizing quantitative amyloid plaque estimation by PET. *Alzheimers Dement.* 2015;11: 1–15.e1-4.
39. Klunk WE, Lopresti BJ, Ikonomovic MD, et al. Binding of the positron emission tomography tracer Pittsburgh compound-B reflects the amount of amyloid-beta in Alzheimer's disease brain but not in transgenic mouse brain. *J Neurosci.* 2005;25: 10598–10606.
40. Klunk WE, Wang Y, Huang GF, et al. The binding of 2-(4′-methylaminophenyl)-benzothiazole to postmortem brain homogenates is dominated by the amyloid component. *J Neurosci.* 2003;23:2086–2092.
41. Lowe VJ, Curran G, Fang P, et al. An autoradiographic evaluation of AV-1451 tau PET in dementia. *Acta Neuropathol Commun.* 2016;4:58.
42. Iqbal K, Alonso Adel C, Chen S, et al. Tau pathology in Alzheimer disease and other tauopathies. *Biochim Biophys Acta.* 2005;1739:198–210.
43. Naseri NN, Wang H, Guo J, Sharma M, Luo W. The complexity of tau in Alzheimer's disease. *Neurosci Lett.* 2019;705:183–194.
44. Aguero C, Dhaynaut M, Normandin MD, et al. Autoradiography validation of novel tau PET tracer ^{18}F-MK-6240 on human postmortem brain tissue. *Acta Neuropathol Commun.* 2019;7:37.
45. Marquié M, Normandin MD, Meltzer AC, et al. Pathological correlations of ^{18}F-AV-1451 imaging in non-Alzheimer tauopathies. *Ann Neurol.* 2017;81: 117–128.
46. Lindberg A, Knight AC, Sohn D, et al. Radiosynthesis, in vitro and in vivo evaluation of ^{18}F-CBD-2115 as a first-in-class radiotracer for imaging 4R-tauopathies. *ACS Chem Neurosci.* 2021;12:596–602.
47. Passamonti L, Vazquez Rodriguez P, Hong YT, et al. ^{18}F-AV-1451 positron emission tomography in Alzheimer's disease and progressive supranuclear palsy. *Brain.* 2017;140:781–791.
48. Whitwell JL, Ahlskog JE, Tosakulwong N, et al. Pittsburgh compound B and AV-1451 positron emission tomography assessment of molecular pathologies of Alzheimer's disease in progressive supranuclear palsy. *Parkinsonism Relat Disord.* 2018;48:3–9.
49. Smith R, Schain M, Nilsson C, et al. Increased basal ganglia binding of ^{18}F-AV-1451 in patients with progressive supranuclear palsy. *Mov Disord.* 2017;32: 108–114.
50. Josephs KA, Murray ME, Tosakulwong N, et al. Tau aggregation influences cognition and hippocampal atrophy in the absence of beta-amyloid: a clinico-imaging-pathological study of primary age-related tauopathy (PART). *Acta Neuropathol (Berl).* 2017;133:705–715.
51. Crary JF, Trojanowski JQ, Schneider JA, et al. Primary age-related tauopathy (PART): a common pathology associated with human aging. *Acta Neuropathol (Berl).* 2014;128:755–766.
52. Jack CR Jr, Wiste HJ, Schwarz CG, et al. Longitudinal tau PET in ageing and Alzheimer's disease. *Brain.* 2018;141:1517–1528.
53. Saade C, Najem E, Asmar K, Salman R, El Achkar B, Naffaa L. Intracranial calcifications on CT: an updated review. *J Radiol Case Rep.* 2019;13:1–18.